Structural and Multidisciplinary Optimization
https://doi.org/10.1007/s00158-019-02482-6

RESEARCH PAPER

Level set topology optimization of cooling channels using the Darcy flow model

Sandilya Kambampati[1] · H. Alicia Kim[1]

Received: 21 August 2019 / Revised: 9 December 2019 / Accepted: 13 December 2019

Abstract
The level set topology optimization method for 2D and 3D cooling channels, considering convective heat transfer for high Reynolds number flows, is presented in this paper. The Darcy potential flow, which is a low-fidelity linear flow model, is used to simulate the flow using the finite element method. The resulting velocity field is used in a convection-diffusion model to simulate the heat transfer using the finite element method. A linear combination of the pressure drop and the average temperature is considered as the objective function, which is minimized subject to a volume constraint and a maximum length scale constraint. The results show that the pressure drop and the average temperature are conflicting criteria, and the trade-off between the two criteria is investigated. We perform a verification study by comparing the Darcy flow field of the obtained optimum designs with that of a high fidelity turbulence model. The verification study shows that there exists a reasonable agreement between the Darcy and the turbulent flow field for narrow channels. Therefore, by restricting the design space to narrow channels, we optimize the cooling performance and sufficiently capture the turbulent flow physics using the low-fidelity Darcy flow model. Finally, we show an example in 3D where we optimize the cooling channel topology that conforms to the surface of a sphere.

Keywords Convective heat transfer · Reynolds Averaged Navier Stokes RANS · Conformal cooling channels · Maximum length scale control

1 Introduction

Heat dissipating devices, such as cooling channels and heat sinks, are typically used in engineering and automotive structures to dissipate heat emanating from batteries, engines, or other heat-generating sources. A common way to dissipate heat is to pass a cooling liquid through the structure. The performance of such cooling systems, in terms of the amount of heat exchanged and the pressure gradient required to pump the fluid, depends on the topology of the cooling channel. Therefore, an efficient cooling channel design is crucial for such heat-dissipating devices.

There has been a lot of research on parametric optimization of cooling channels. In such parametric optimization methods, the channel path is defined by a set of parameters in a predefined layout. In Qiao (2006), a 2D pipe section optimization design is presented, where the channel is described by parameters such as size and location, and a novel hybrid optimizer based on the Davidon–Fletcher–Powell method and simulated annealing is used. Tan et al. (2016) used a set of control points to define the channel paths, and used gradient-based shape optimization to optimize the cooling performance of microchannels to be embedded in microvascular composites. The design studies of cooling channels that conform to a given surface are of a great interest in plastic injection moulding (Dimla et al. 2005). The particle swarm method is used to optimize the heating/cooling channels for rapid heat cycle molding with hot medium heating and coolant cooling in Wang et al. (2011), where the diameters and the distances of the cooling channels from cavity surfaces are used as design variables. In Hu et al. (2016), the cooling performance of

Responsible Editor: Ole Sigmund

Electronic supplementary material The online version of this article (https://doi.org/10.1007/s00158-019-02482-6) contains supplementary material, which is available to authorized users.

✉ Sandilya Kambampati
sakambampati@ucsd.edu

H. Alicia Kim
alicia@ucsd.edu

[1] Structural Engineering, University of California San Diego, San Diego, CA, 92093, USA

Published online: 11 February 2020

3D cooling channel designs such as longitudinal, transversal, parallel, and serpentine conformal cooling channels are investigated. However, such parametric optimization methods do not allow introducing new channels between pre-defined channels, and the optimized channel path is heavily dependent on the initial parameterized layout.

Topology optimization, on the other hand, is an innovative design tool that can help with designing cooling channels while overcoming the limitations of the parametric optimization methods. Typical topology optimization methods of cooling channels involve flow simulation models to compute fluid velocity and pressure fields, and convective heat transfer simulation models based on the fluid velocity. Topology optimization considering high-fidelity turbulent models for 2D problems is presented in Yoon (2016), and for 3D models is presented in Dilgen et al. (2018a, b). Such high-fidelity turbulent models involve solving nonlinear partial differential equations and are computationally expensive to solve. Therefore, a lower fidelity model that can reasonably approximate the high-fidelity turbulence model is attractive in conceptual design studies using topology optimization.

Topology optimization using lower fidelity models for fluid flow can be found in literature. Topology optimization of fluids using Stokes flow, which is used to model flow with low Reynolds numbers, is presented in Borrvall and Petersson (2003). In Gersborg-Hansen et al. (2005), topology optimization was applied to low-to-moderate Reynolds number flow between flat plates. Guest and Prévost (2006) developed a Darcy-Stokes finite element method for topology optimization. The design of a heat-dissipating structure using topology optimization is presented in Yoon (2010), by modeling the steady state Navier-Stokes equations and convective heat transfer. In Yaji et al. (2015), Yaji et al. presented a level set–based topology optimization method to design cooling channels by using the Tikhonov-based regularization scheme to control the geometry of the structure.

A laminar flow model is used to design conformal cooling channels for 3D printed plastic injection moulds in Jahan et al. (2019) and Wu and Tovar (2018). In Zhao et al. (2019), a topology optimization method is presented to design straight channel cooling structures for efficient heat transfer and load carrying capabilities, by assuming a constant velocity of the channels. Recently, a Darcy potential flow model for density-based topology optimization is proposed by Zhao et al. (2018), for designing cooling channels at high Reynolds numbers. They showed that the Darcy flow model is a viable alternative to a turbulent flow model in the design of well-performing cooling channels. The approach presented by Zhao et al. has been extended to the topology optimization for natural convection problems in Asmussen et al. (2019) and Pollini et al. (2020). However, Zhao et al. did not discuss the trade-off between the pressure drop across the channel and the cooling performance of the topology. They also did not impose any constraints on the maximum width of the optimized channels, which can play a key role in avoiding recirculation in the flow, as we show in this paper. Moreover, they investigated only 2D optimization problems and did not explore 3D design spaces.

In this paper, we present a new level set topology optimization method for 2D and 3D problems considering convective heat transfer, for high Reynolds number flows. The Darcy potential flow model (Zhao et al. 2018) is used to compute the flow characteristics. With the help of the resulting fluid flow, the heat transfer is modeled by the convection-diffusion equation using the finite element (FE) method. The objective function which is a linear combination of the pressure drop and the average temperature is minimized subject to a volume constraint and a maximum length scale constraint. The trade-off between the pressure drop and the average temperature is discussed. We perform a verification study by comparing the Darcy flow field of the optimized designs with that of a turbulent flow field for the same designs. The verification study shows that there exists a reasonable agreement between the Darcy and the RANS flow fields only when the width of the channels is small. By restricting the design space to narrow channels, we are able to optimize the cooling performance and sufficiently capture the turbulent flow physics using the low fidelity Darcy flow model. Finally, we optimize conformal cooling channels on the surface of a sphere, where we show that the optimized channels branch out from the inlets, distribute themselves efficiently on the surface of the sphere in such a way that the average temperature of the sphere is reduced.

2 Optimization method

In this study, we use the Darcy potential flow model to simulate the flow. The resulting fluid flow is used in a convection-diffusion equation to simulate the heat transfer. This model is extensively presented in Zhao et al. (2018). We use the level set method for the topology optimization and the adjoint method is used to compute sensitivities. A detailed description of the models developed are presented in this section.

2.1 Level set method

The level set method (LSM) is employed for topology optimization. The boundary of the structure is described by an implicit function $\phi(x)$, which is defined as

$$\begin{aligned} \phi(x) &\geq 0, \ x \in \Omega \\ \phi(x) &= 0, \ x \in \Gamma \\ \phi(x) &< 0, \ x \notin \Omega \end{aligned} \tag{1}$$

where Ω is the domain, and Γ is the domain boundary. The boundary of the structure is changed implicitly through $\phi(x)$. This way of representing the domain allows the boundary to change under a given velocity field $V_n(x)$. The level set $\phi(x)$ is updated using the level set equation, which is a type of a Hamilton-Jacobi equation given by Sethian and Vladimirsky (2000),

$$\frac{d\phi(x)}{dt} + |\nabla\phi(x)|V_n(x) = 0, \tag{2}$$

which is discretized and solved numerically using the following equation (Sethian 1999),

$$\phi_j^{k+1} = \phi_j^k - \Delta t|\nabla\phi_j^k|V_{n,j} \tag{3}$$

where j is a discrete point in the domain, and $|\nabla\phi_j|$ is computed using the Hamilton-Jacobi weighted essentially non-oscillatory (HJ-WENO) scheme (Sethian and Vladimirsky 2000).

A schematic of our level set topology optimization method is shown in Fig. 1. For a given topology, the boundary is extracted as a collection of boundary points, and the fractions of the elemental volume cut by the level set for all the FE mesh elements are computed. This is followed by an FE analysis and element centroid sensitivity computation. The boundary point sensitivities are computed from the element centroid sensitivities using the least squares interpolation. Using the sensitivities, the boundary point velocities are then optimized using mathematical programming. The level set function is then updated using the boundary point velocity field. This process is repeated until convergence is reached. Further details of our level set topology optimization can be found in Dunning and Kim (2015).

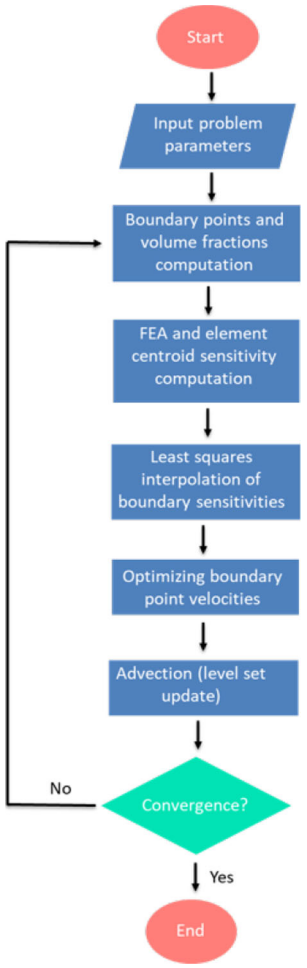

Fig. 1 A schematic of the level set method used for topology optimization

2.2 Fluid flow model

In this section, we briefly describe the flow modeled using the finite element method. A common model used to describe a flow is the incompressible steady state Navier-Stokes equations

$$\rho u \cdot \nabla u = -\nabla p + \mu\nabla^2 u \tag{4}$$

$$\nabla \cdot u = 0 \tag{5}$$

where ρ is the density, u is the velocity of the fluid, p is the pressure, and μ is the dynamic viscosity. The above Navier-Stokes equations are non-linear equations, and typically turbulence models such as Reynolds-Averaged Navier-Stokes (RANS) simulations are used to model this flow, as the determination of the length scales of the flow in the domain is challenging in topology optimization. However, RANS simulations are computationally expensive. A viable alternative to the RANS model for capturing the flow physics inside cooling channels is to use the Darcy potential flow (Zhao et al. 2018), which assumes the velocity to be proportional to the gradient of pressure as

$$u = -\frac{\kappa}{\mu}\nabla p \tag{6}$$

where κ is the permeability of the fluid. Equation 6 is substituted in the continuity equation in Eq. 5 yielding

$$\nabla \cdot (\frac{\kappa}{\mu}\nabla p) = 0 \tag{7}$$

The Darcy potential flow is a low-fidelity model that (a) assumes the flow to be irrotational, (b) does not include the non-linear inertia term, and (c) can be modeled using Eq. 7, which is is a linear, elliptic partial differential equation, which is significantly easier to compute than the RANS equations. The motivation for using the Darcy flow to compute the flow field comes from the fact that the pressure gradient is approximately constant in long channels, and the velocity in the channel is proportional to the pressure gradient. Therefore, by appropriately selecting the permeability constant of the fluid κ, we can sufficiently

capture the flow physics in channel flow using the Darcy potential flow.

The finite element method is used to model the Darcy potential flow equation in Eq. 7 resulting in the following equation:

$$K_p P = F_p \tag{8}$$

where N_e is the number of elements, K_p is the permeability matrix, given by

$$K_p = \sum_i^{N_e} K_{p,i}^e \tag{9}$$

$K_{p,i}^e = \kappa_i / \mu K_{p,0}^e$ is the elemental permeability matrix. and

$$K_{p,0}^e = \int_{\Omega_i} B^T B d\Omega \tag{10}$$

is the homogeneous elemental permeability matrix, $B = \nabla N$ is the gradient of the shape functions N, and

$$\kappa_i = \kappa_s + (\kappa_f - \kappa_s) x_i \tag{11}$$

where x_i is the fraction of the elemental volume cut by the level set, κ_s and κ_f are the permeability values of the solid and fluid, respectively, and Ω_i is the domain of the element i. The right hand side of Eq. 8, F_p is given by

$$F_p = \int_\Gamma N^T (n \cdot u_{in}) d\Gamma \tag{12}$$

where u_{in} is velocity of the flow at the flow inlet, and n is the normal vector to the boundary.

2.3 Heat transfer model

Based on the fluid velocity u, the heat transfer can be modeled using the following convection-diffusion equation

$$\rho c_p u \cdot \nabla T = k \nabla^2 T + Q \tag{13}$$

where c_p is the specific heat, k is the conductivity coefficient, T is temperature, and Q is the heat generation rate. The finite element analysis can be used to model Eq. 13 numerically as

$$(K_t + C) T = F_t \tag{14}$$

where K_t is the conductivity matrix, C is the convection-matrix, and F_t is the thermal load. The conductivity matrix K_t is approximated by

$$K_t = \sum_i^{N_e} K_{t,i}^e = \sum_i^{N_e} k_i K_{t,0}^e \tag{15}$$

where k_s is the conductivity of the solid, k_f is the conductivity of the fluid, and $K_{t,0}^e$ is the homogeneous elemental conduction matrix is given by

$$K_{t,0}^e = \int_{\Omega_i} B^T B d\Omega \tag{16}$$

and k_i is the interpolated elemental conductivity coefficient, given by

$$k_i = (k_s + (k_f - k_s) x_i) \tag{17}$$

The convection matrix C is assembled using the following elemental convection matrix C^e, given by

$$C = \sum_i^{N_e} C^e = \sum_i^{N_e} \rho_i c_{p,i} \kappa_i C_0^e \tag{18}$$

where ρ_i and $c_{p,i}$ are interpolated elemental density and specific heat coefficient, given by

$$\rho_i = \rho_s + (\rho_f - \rho_s) x_i \tag{19}$$

$$c_{p,i} = c_{ps} + (c_{pf} - c_{ps}) x_i \tag{20}$$

where ρ_s and ρ_f are the densities of the solid and fluid, respectively, c_{ps} and c_{pf} are the specific heat coefficients of the solid and fluid, respectively, and C_0^e is the homogeneous elemental convection matrix given by

$$C_0^e = \int_{\Omega_i} -\hat{N}^T (\frac{1}{\mu} B p_e)^T B d\Omega \tag{21}$$

where p_e are the pressure values at the element nodes, and $\hat{N}$ includes the streamline upwind stabilization term given by

$$\hat{N} = N + \frac{h_e}{2} \left(\frac{u}{\|u\|} \right) B \tag{22}$$

where h_e is the width of an element.

2.4 Maximum length scale control

Length scale control is not automatically built into the level set method. We briefly discuss the methodology for imposing a maximum length scale constraint in the optimization here. This formulation is presented and extensively discussed in Wu et al. (2017) for designing porous structures. In this study, we use the same formulation to impose a maximum allowable channel width. Specifically, we define $\bar{x}_i$ to be the average of the volume fractions of the design around an element i inside the radius r_{max} as

$$\bar{x}_i = \frac{\sum_j I(i,j) x_j}{\sum_j I(i,j)} \tag{23}$$

where $I(i,j)$ is an indicator function defined as

$$\begin{aligned} I(i,j) &= 1; d(i,j) \leq r_{max} \\ I(i,j) &= 0; d(i,j) > r_{max} \end{aligned} \tag{24}$$

where $d(i, j)$ is the distance between the centroids of elements i and j. For the maximum width of the channels to be less than r_{max}, $\bar{x}_i$ should be less than unity for all the elements, given by

$$\max_{\forall i} \bar{x}_i < 1 \tag{25}$$

In this study, we use the p-norm function to approximate the maximum of $\bar{x}_i$ as

$$\bar{x}_{max} = \max_{\forall i} \bar{x}_i \approx \|\bar{x}_i\|_p = \left[\sum_i \bar{x}_i^p\right]^{\frac{1}{p}} \tag{26}$$

The derivative of $\bar{x}_{max}$ w.r.t. the volume fraction x_i is approximated as

$$\bar{s}_i = \frac{d\bar{x}_{max}}{dx_i} \approx \frac{x_{max}}{\|\bar{x}_i\|_p} \frac{\|\bar{x}_i\|_p^{1-p}}{p} \sum_j p\bar{x}_j^{p-1} I(i, j) \tag{27}$$

In this study, we set $p = 8$.

2.5 Optimization problem definition

In this study, we use the weighted multi-objective approach to minimize the average temperature T_{av} and the pressure drop P_d across the inlet and outlet of the flow, corresponding to a volume constraint. Such weighted multi-objective approaches are used for convective heat transfer based topology optimization for design space exploration in Koga et al. (2013) and Kontoleontos et al. (2013). The objective function F is given by

$$F = w\frac{T_{av}}{T_0} + (1 - w)\frac{P_d}{P_0} = f_1^T T + f_2^T P \tag{28}$$

where f_1 is a constant vector with each element having a value of $w/(T_0 N_n)$, and N_n is the number of FE nodes. f_2 is a vector where all elements of f_2 are set to zero except for the ith node where i is a degree of freedom corresponding to the flow inlet, with the corresponding values set to $(1 - w)/(P_0 N_o)$, where N_o is number of nodes that belong to the inlet. w and $1 - w$ are the weights corresponding to the pressure drop and average temperature, respectively, and P_0 and T_0 are the reference pressure and temperature. The optimization problem can be now stated as

$$\begin{aligned} \min_{\Omega} \quad & F = f_1^T T + f_2^T P \\ \text{s.t.} \quad & V \le V_0 \\ & K_p P = F_p \\ & (K_t + C)T = F_t \\ & \bar{x}_{max} < 1 \end{aligned} \tag{29}$$

where Ω is the topology of the cooling channels, and V and V_0 are the volume and volume constraint, respectively.

2.6 Sensitivity analysis

In this section, the computation of boundary point sensitivities for the weighted multi-objective function defined in Eq. 28 is presented. First, the sensitivities are calculated at the centroids of the elements from which the sensitivities at the boundary points are computed using the least squares interpolation (Dunning et al. 2011).

The adjoint method is used to compute the sensitivity of the objective function. The Lagrangian $\mathcal{L}$ for the objective function and the equilibrium equations of flow and temperature defined in Eq. 29 is

$$\mathcal{L} = f_1^T T + f_2^T P - \lambda_t^T((K_t + C)T - F_t) - \lambda_p^T(K_p P - F_p) \tag{30}$$

where λ_t and λ_p are the adjoint variables corresponding to the temperature and flow variables. The adjoint variable λ_t is computed by solving $\frac{\partial \mathcal{L}}{\partial T} = 0$, which yields

$$(K_t^T + C^T)\lambda_t = f_1 \tag{31}$$

The adjoint variable λ_p is computed by solving $\frac{\partial \mathcal{L}}{\partial P} = 0$, resulting in

$$K_p \lambda_p = f_2 - T^T \frac{\partial C}{\partial P}\lambda_t \tag{32}$$

Note that the term $\frac{\partial C}{\partial P}$ appears in Eq. 32 because the convection matrix depends on the flow velocity.

The Lagrangian function $\mathcal{L}$ can be differentiated with respect to the volume fraction x_i of an element i to compute the sensitivity at the centroid s_i as follows

$$\begin{aligned} s_i &= \frac{\partial \mathcal{L}}{\partial x_i} \\ &= \frac{\partial}{\partial x_i}\left(f_1^T T + f_2^T P - \lambda_t^T((K_t + C)T - F_t) - \lambda_p^T(K_p P - F_p)\right) \\ &= -\lambda_t^T\left(\frac{\partial K_t}{\partial x_i} + \frac{\partial C}{\partial x_i}\right)T - \lambda_p^T \frac{\partial K_p}{\partial x_i} P \\ &= -(k_f - k_s)\lambda_{t,i}^{eT} K_{t,0}^e T_i^{eT} \\ &\quad -\left[\rho_i c_{p,i}(\kappa_f - \kappa_s) + \kappa_i c_{p,i}(\rho_f - \rho_s) + \rho_i \kappa_i (c_{pf} - c_{ps})\right]\lambda_{t,i}^{eT} C_0 T_i^{eT} \\ &\quad -(\kappa_f - \kappa_s)\lambda_{p,i}^{eT} K_{p,0}^e P_i^{eT} \end{aligned} \tag{33}$$

Next, the boundary sensitivity s_j^b of a boundary point j is computed using the least squares interpolation based on the centroid sensitivities of the neighboring elements. As an illustrative example, the schematic of the boundary point of interest and the surrounding elements in 2D is shown in Fig. 2. All the elements which lie inside a support radius (shown in red) of the boundary point are collected. The following function is fitted to compute the boundary sensitivity of the point.

$$f_j(x, y) = a_0^j + a_1^j(x - x_j) + a_2^j(y - y_j) \tag{34}$$

where (x_j, y_j) are the coordinates of the the boundary point j. The coefficients (a_0^j, a_1^j, a_2^j) are computed such that the least squares error of the sensitivities at the element centroids inside the support radius is minimized. Finally, the sensitivity of the boundary point s_j^b is given by

$$s_j^b = f_j(x_j, y_j) = a_0^j \tag{35}$$

This process is performed for all the boundary points to compute the sensitivities.

2.7 Optimization

In this section, we show the details of the algorithm that computes the optimum scalar velocity field V_n of the boundary. The objective and constraint functions in Eq. 29 are linearized with the help of the sensitivities. The optimum velocity of the boundary points $V_{n,j}$, which is required to advect the level set function ϕ, is computed by solving the following optimization problem.

$$\begin{aligned} \min_{V_{n,j}} \quad & \Delta F = \textstyle\sum_j (s_j^b A_j V_{n,j}) \Delta t \\ \text{s.t.} \quad & V = V_c + \textstyle\sum_j (V_j A_j V_{n,j}) \Delta t \le V_t \\ & \bar{x}_{max} = \bar{x}_{max,c} + \textstyle\sum_j (\bar{s}_j A_j V_{n,j}) \Delta t \le \bar{x}_{max,t} \\ & l_j \le V_{n,j} \le u_j \end{aligned} \tag{36}$$

where $V_j = -1$ the sensitivity of the volume constraint, A_j is the average area of all the polygons that have this current boundary point as a vertex, $\Delta t = 1$ is the pseudo time step, l_j is the lower bound, and u_j is the upper bound. V_t and $\bar{x}_{max,t}$ are the target constraints imposed for the current iteration, given by

$$\begin{aligned} V_t &= \max(V_0, V_c + \sum_j (\gamma V_j A_j l_j) \\ \bar{x}_{max,t} &= \max(1, \bar{x}_{max,c} + \sum_j (\gamma \bar{s}_j A_j l_j) \end{aligned} \tag{37}$$

where V_c and $\bar{x}_{max,c}$ are the volume and $\bar{x}_{max}$ for the current iteration, respectively, and γ is the constraint relaxation factor. When $\gamma = 1$, the optimizer tries to satisfy the volume constraint without regard to the objective function. On the other hand, when $\gamma = 0$, the optimizer tries to minimize the objective function without regard to satisfying the volume constraint. In this study, we set $\gamma = 0.5$, which serves as a compromise between satisfying the constraint and minimizing the objective function.

The linear programming in Eq. 36 is solved using the Simplex method (Arora 2004), and the optimum velocities $V_{n,j}$ are used to update the level set function using the level set (2). This process is iterated until a convergence is obtained.

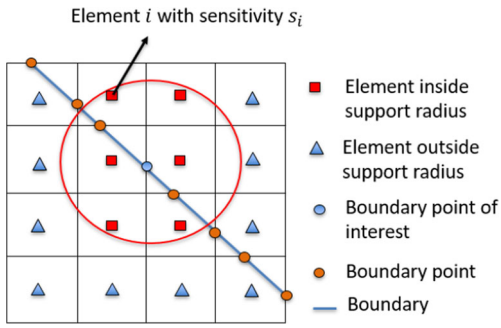

Fig. 2 Interpolation of boundary sensitivities from element sensitivities

Table 1 Material properties for steel and water

	Water	Steel
Conductivity (k, $W/m/K$)	0.6	44.0
Specific heat (c_p, J/kg/K)	4200.0	460.0
Density (ρ , kg/m^3)	1000.0	7800.0
Viscosity (μ, Pa s)	0.001	0.001

3 Numerical examples

In this section, numerical examples of the mathematical models presented in the previous section and their application in level set topology optimization of cooling channels for different examples in 2D and 3D are presented. The fluid is assumed to be water and the solid is assumed to be steel. The properties of water and steel are tabulated in Table 1.

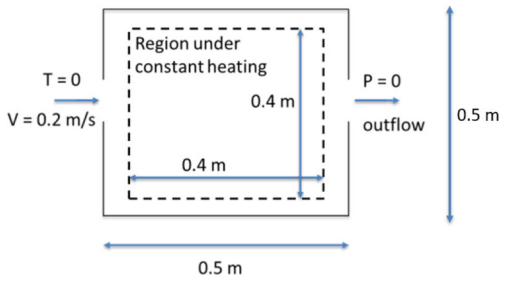

Fig. 3 A schematic of a domain subject to uniform heating, with flow entering from the left side and exiting through the right side

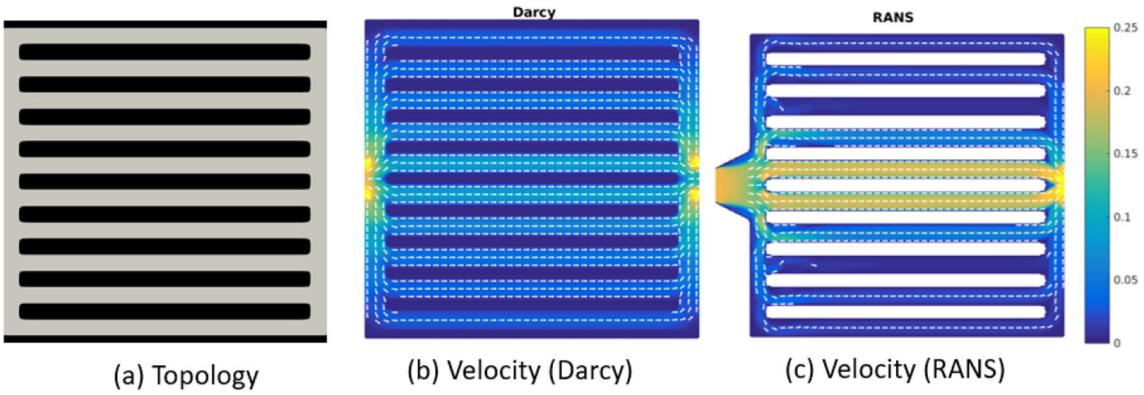

Fig. 4 **a** Topology of the baseline design. **b** The velocity field in m/s computed by the Darcy flow model. **c** The velocity field in m/s computed by the RANS model

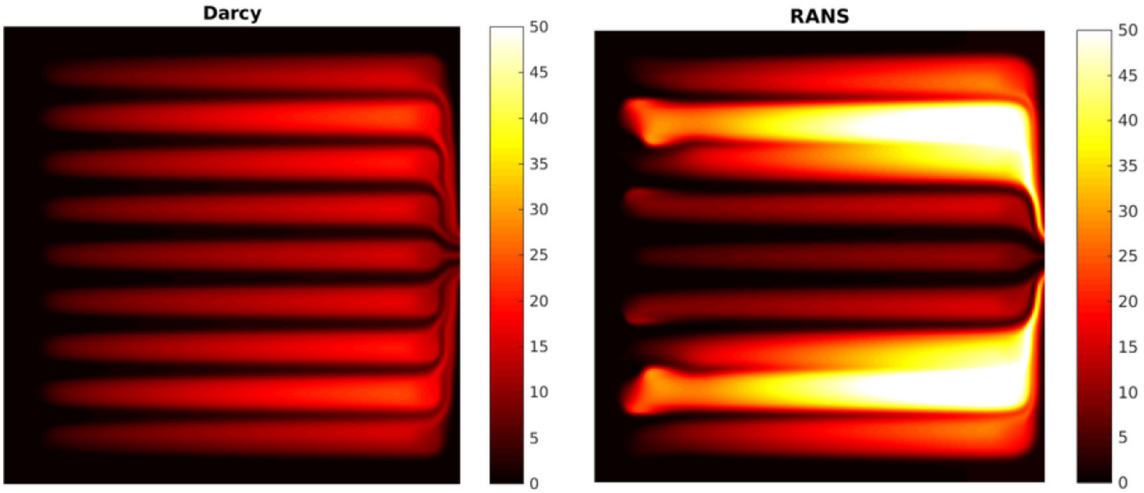

Fig. 5 The temperature field (in °C) computed using the Darcy and RANS flow fields

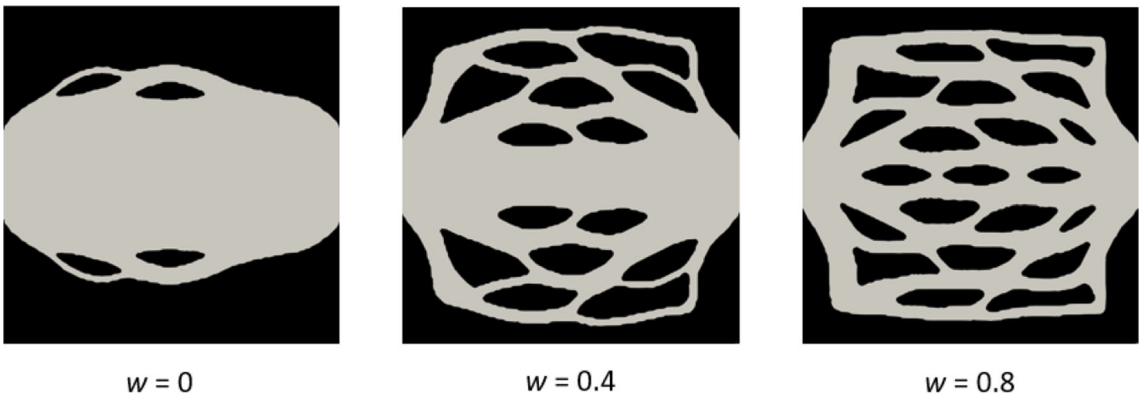

Fig. 6 Optimized cooling channel designs obtained obtained without using the length scale constraint for different values of w, the weight corresponding to temperature. This figure shows that as w increases, the channels spread out and the number of channels also increases

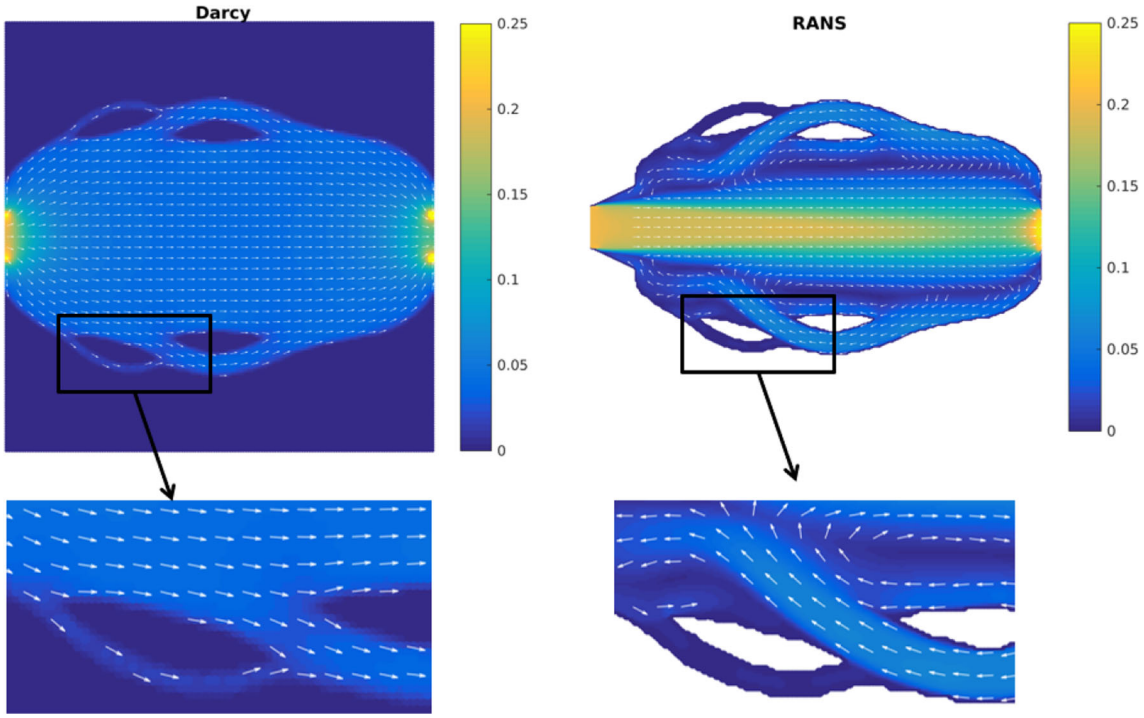

Fig. 7 Comparison between the velocity fields (in m/s) computed by Darcy and RANS flow models for the topology obtained with $w = 0$. The RANS flow model predicts recirculation in the outer channels, where the flow velocity is towards the inlet. The Darcy flow model does not predict recirculation. This figure shows a significant discrepancy between the Darcy and RANS flow fields

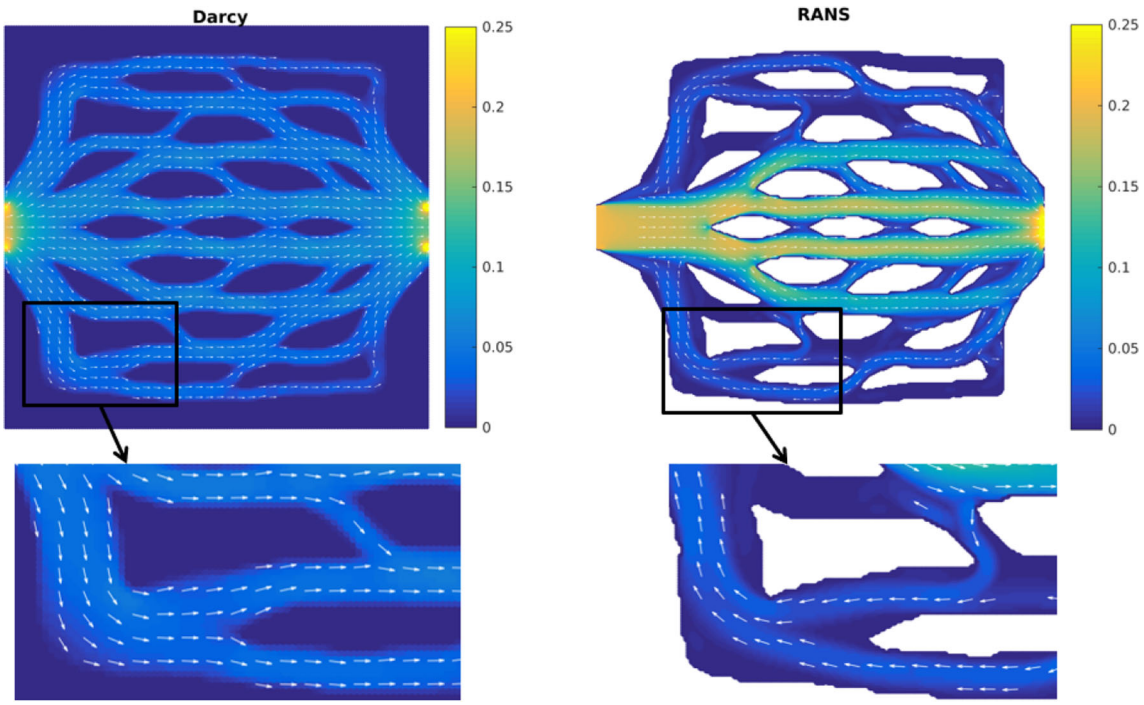

Fig. 8 Comparison between the velocity fields (in m/s) computed by Darcy and RANS flow models for the topology obtained with $w = 0.8$. The RANS flow model predicts recirculation in the outer channels, where the flow velocity is towards the inlet. The Darcy flow model does not predict recirculation. This figure shows a significant discrepancy between the Darcy and RANS flow fields

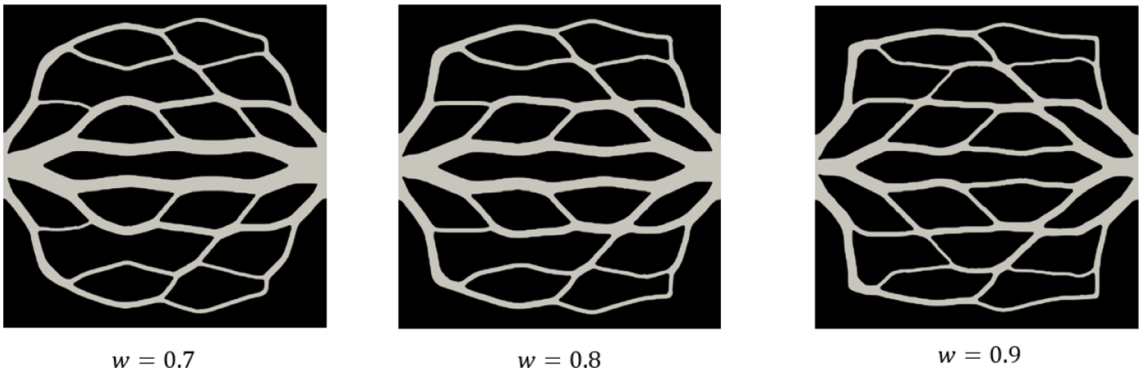

Fig. 9 Optimized cooling channel designs obtained without using a length scale constraint and a volume constraint $V_0 = 20\%$ for different values of w, the weight corresponding to temperature

3.1 2D cooling channel design

In this section, topology optimization of 2D cooling channels is presented. A schematic of the domain and boundary conditions of the flow entering through the inlet on left hand side (0.05 m wide) at $V = 0.2$ m/s and exiting through the outlet on the right hand side (0.05 m wide) is shown in Fig. 3. The domain is subjected to a constant heating of $Q = 2000$ kW/m^3. The boundary conditions are $T = 0$ at the fluid entry region and $P = 0$ at the fluid exit region. The FE mesh is discretized into 160 × 160 elements. The reference pressure $P_0 = 10$ Pa and the reference temperature $T_0 = 10$ °C. The volume constraint $V_0 = 50\%$. The Reynolds number of the flow, computed based on the inlet channel width is 10^4.

3.1.1 Baseline design

Figure 4 a shows the topology of the baseline design chosen for this study. It has ten parallel horizontal channels that are equidistant from each other, connected to each other through two vertical channels near the inlet and the outlet.

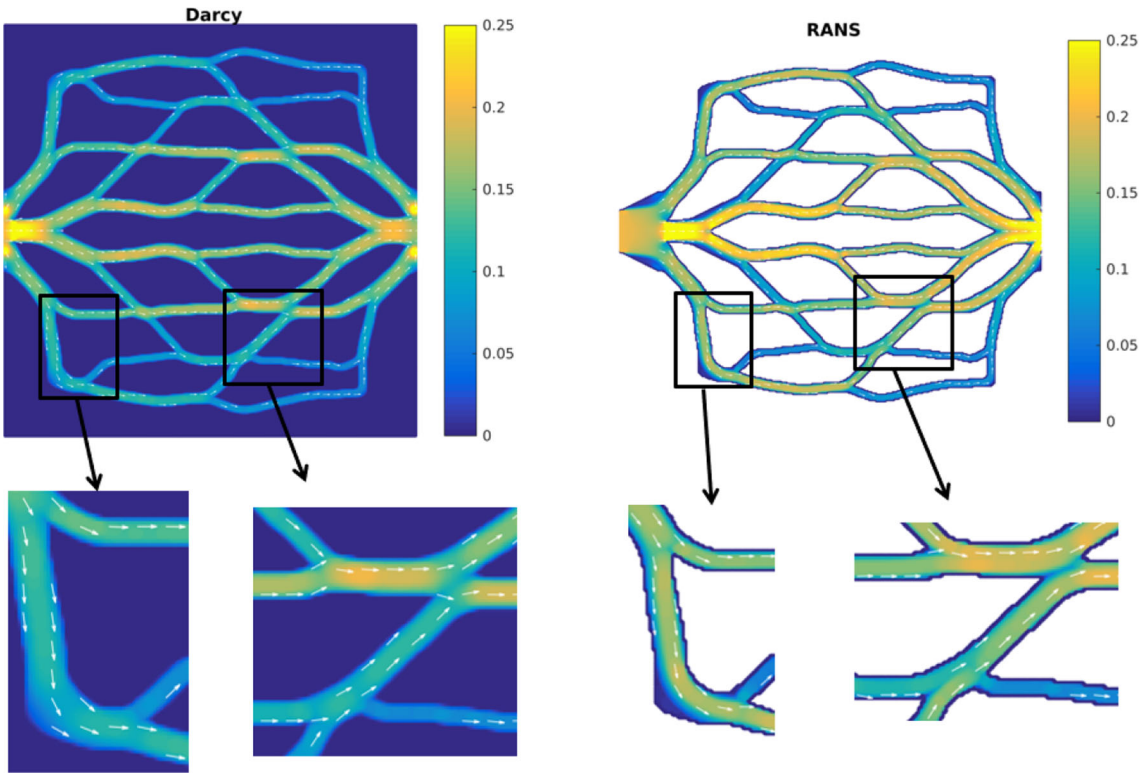

Fig. 10 Comparison between the velocity fields (in m/s) computed by Darcy and RANS flow models without using a length scale constraint and a volume constraint $V_0 = 20\%$, for the topology obtained with $w = 0.9$

Figures 4 b and c show the velocity distribution computed using the Darcy model and RANS model, respectively. The RANS model was simulated using Ansys Fluent. An inlet channel is added for the RANS model for the flow to fully develop. From Fig. 4c, we can see that for the RANS flow, the magnitude of the velocity is high in the channels close to the center and low in the channels away from the center. On the other hand, from Fig. 4b, we can see that the velocity is more evenly distributed across the channels for the Darcy flow. The permeability constant for the Darcy flow model is adjusted by trial and error to $\kappa = 1.9 \times 10^{-6}$ so that the pressure drop predicted by the Darcy flow model and the RANS model are the same for the baseline model.

Figure 5 shows the temperature distribution of the domain simulated using the RANS model and the Darcy flow model. The velocity field computed using the RANS model in Ansys Fluent is used in the conduction-convection model developed in-house to compute the temperature field. We can see that the RANS model predicts low temperature in the regions near the centerline and high temperatures in regions away from the centerline. The Darcy model, on the other hand, predicts a more uniform distribution of temperature across the domain. The average temperature predicted by the RANS model and the Darcy model are 14.5 °C and 6.7 °C, respectively. Thus, the Darcy model under-predicts the average temperature and over-predicts the heat transfer due to the more evenly distributed flow field.

3.2 Optimized results without using length scale control

The optimization is performed for the weight corresponding to the pressure drop and the average temperature, for $w = 0, 0.4$, and 0.8 in Eq. 28, a volume constraint $V_0 = 50\%$, and without using the maximum length scale constraint. The optimized topologies are shown in Fig. 6. We can see for low values of w, the objective function is given more weight to the pressure drop than the temperature. When $w = 0$, the optimized design has a wide channel going through the center—thus minimizing the distance the fluid travels from the inlet to the outlet. As w increases, the channel along the center gets narrower, and bifurcates into an increasing number of sub-channels, thus increasing the areas that the cooling flow reaches. Furthermore, the channels are distributed in such a way that the fluid enters the domain, travels to greater regions in the domain, drawing heat from the solid while it travels, and exits through the outlet.

In Fig. 7, we show the velocity field of the topology obtained for $w = 0$ shown in Fig. 6, using Darcy flow and RANS model. As we can see from Fig. 7 there is a significant discrepancy between the velocity field predicted using the Darcy flow model and the RANS model. Specifically, the Darcy flow model predicts that the flow is evenly distributed across the domain. The RANS model, on the other hand, predicts that most of the flow is travelling close to the centerline. Moreover, the RANS model predicts flow recirculation in the outer channels, where the flow travels toward the inlet. The presence of recirculation drastically decreases the efficiency of the cooling channel. As a result, the average temperature predicted by the RANS model is a high, 840.7 °C. On the other hand, since the Darcy flow model predicts a more uniform distribution of velocity and no recirculation, the average temperature predicted is a low, 52.9 °C.

The discrepancy between the Darcy flow model and the RANS model is also observed for other values of w. In Fig. 8, we show the velocity field of the topology obtained for $w = 0.8$ (shown in Fig. 6), using Darcy flow and RANS model. The Darcy flow model predicts that the flow is more

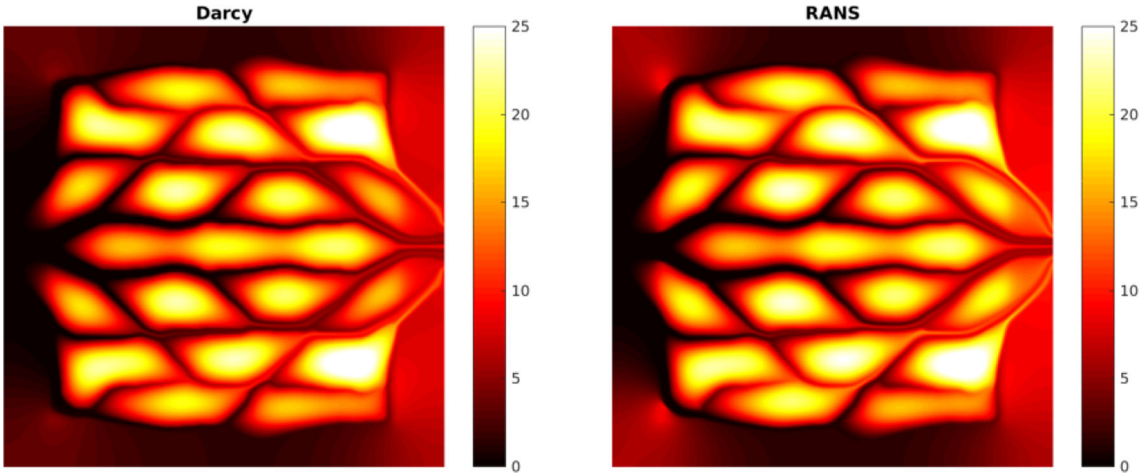

Fig. 11 The temperature field (in °C) computed using the Darcy and RANS flow fields for the topology obtained without using a length scale constraint and a volume constraint $V_0 = 20\%$ with $w = 0.9$. This figure shows very little difference in the temperature fields

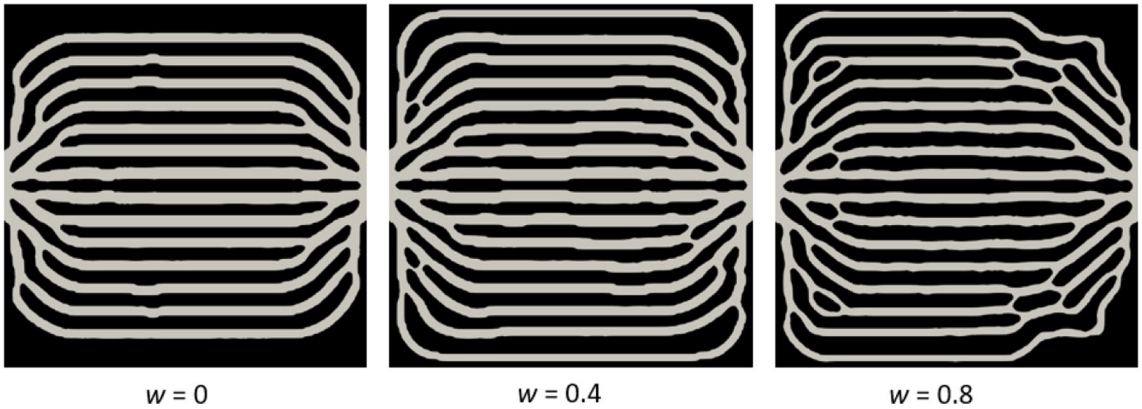

Fig. 12 Optimized cooling channel designs obtained using a channel width constraint of 3.12 cm for different values of w, the weight corresponding to temperature

evenly distributed across the channel domain. The RANS model, on the other hand, predicts that most of the flow is travelling through the channel close to the centerline. Furthermore, the RANS model predicts flow recirculation in the outer channels, where the flow travels toward the inlet. As a result, the average temperature predicted by the RANS model is a high, 134.9 °C. On the other hand, since the Darcy flow model predicts a more uniform distribution of velocity and no recirculation, the average temperature predicted is a low, 5.0 °C.

Figures 7 and 8 show that the average temperature computed from velocity fields predicted by the Darcy flow and RANS are not in agreement—with over an order of magnitude difference in the values. However, for the baseline design shown in Fig. 4, the difference in the computed temperature (Darcy flow vs RANS) is not as severe (6.7 °C vs 14.5 °C) as the temperature difference computed for the optimized results. Observing the baseline topology and the optimized topologies, we hypothesize that, since the baseline topology comprises of narrower channels than the optimized topologies, the channel width plays a key role in assessing the discrepancy between the Darcy flow and RANS velocity fields.

Next, we investigate the effects of a lower value of the volume constraint. The optimized topology obtained without using a maximum length scale constraint, for a

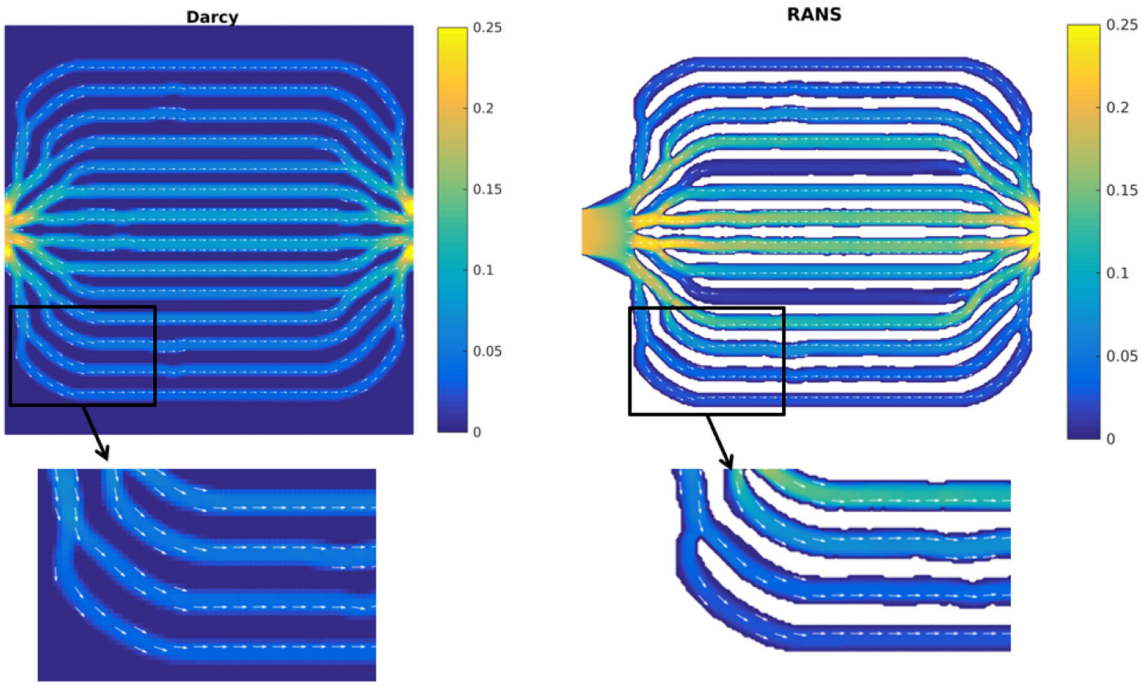

Fig. 13 Comparison between the velocity fields (in m/s) computed by Darcy and RANS flow models for the topology obtained with $w = 0$ and a maximum channel width constraint of 3.12 cm. The RANS and Darcy flow models predict no recirculation in the channels

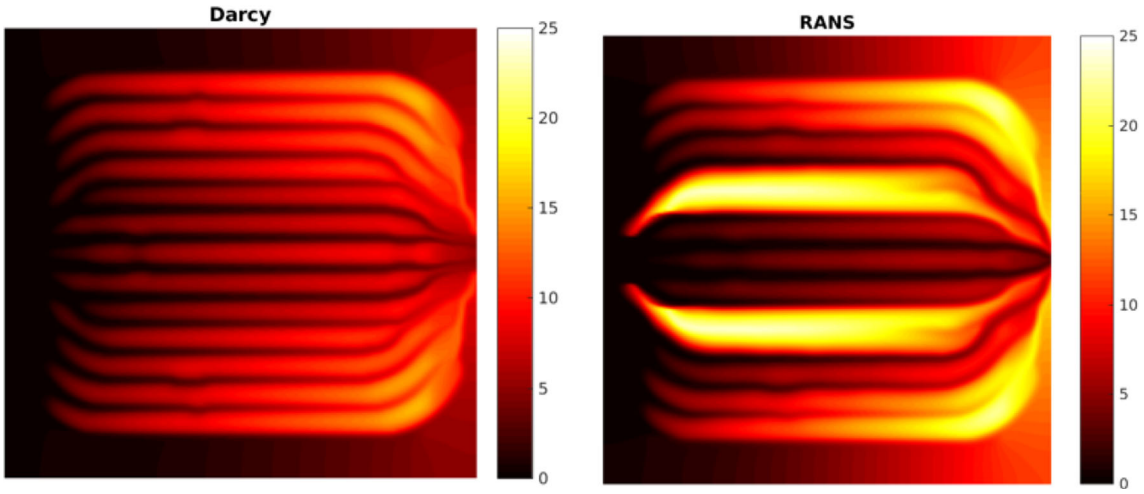

Fig. 14 The temperature field (in °C) computed using the Darcy and RANS flow fields

volume constraint $V_0 = 20\%$ and $w = 0.7, 0.8$, and 0.9 is shown in Fig. 9. We can see from Fig. 9 that the optimized topologies features narrower channels. The velocity field for the topology obtained for $w = 0.9$ is shown in Fig. 10, where we can see that there is no recirculation in the channels. The average pressure predicted by the Darcy flow and RANS models are 55.3 Pa and 65.4 Pa, respectively, with the error being approximately 18%. The temperature field computed using the Darcy flow and RANS models is shown in Fig. 11, where we can see that there is very little difference in the temperature fields. The average temperature computed by the Darcy flow and RANS models are 8.5 °C and 9.3 °C, with the error being approximately 9%.

3.3 Optimized results with using length scale control

In this section, we discuss the methodology for obtaining narrow channels—by using a maximum length scale constraint. Specifically, the optimization results are obtained

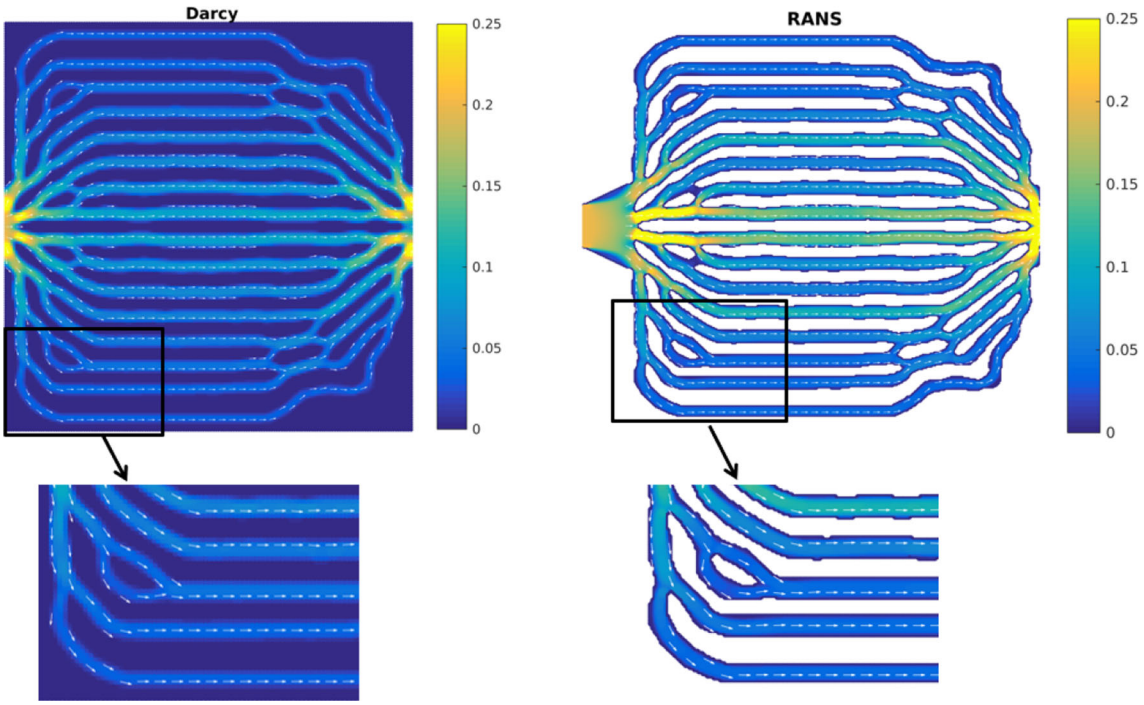

Fig. 15 Comparison between the velocity fields (in m/s) computed by Darcy and RANS flow models for the topology obtained with $w = 0.8$ and a maximum channel width constraint of 3.12 cm. The RANS and Darcy flow models predict no recirculation in any of the channels

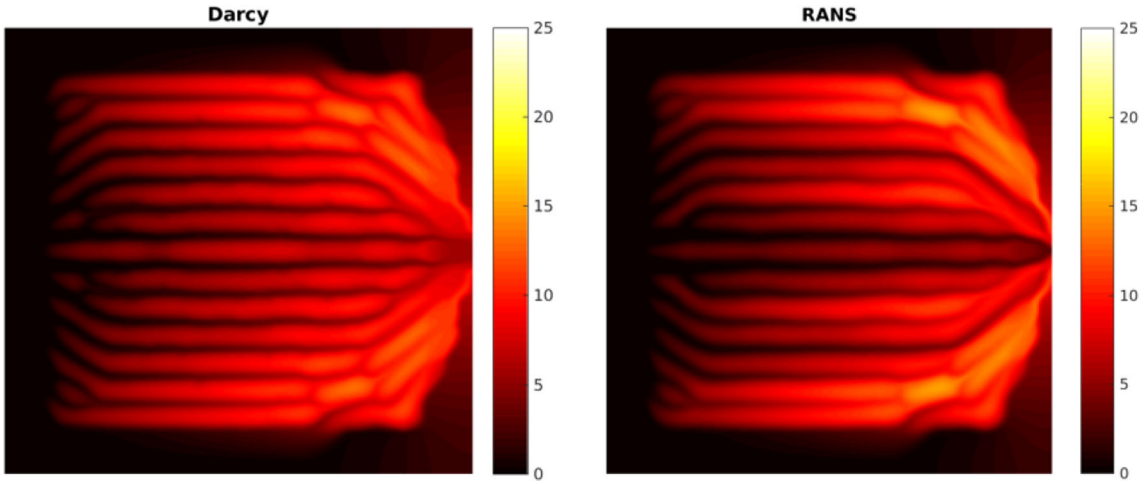

Fig. 16 The temperature field (in °C) computed using the Darcy and RANS flow fields, showing very little difference in the temperature fields

using a maximum length scale of $r_{max} = 3.12$ cm (equivalent to the width of 10 elements), and a volume fraction $V_0 = 50\%$. Figure 12 shows the results obtained for $w = 0, 0.4$, and 0.8. From Fig. 12, we can see that all the channels are narrower compared with the topologies obtained when the maximum length scale was not used for the same volume constraint (i.e., designs presented in Fig. 6). Furthermore, we can see that for $w = 0$, there are exactly 14 distinct horizontal channels in the optimized design. For $w = 0.8$, there are 16 distinct horizontal channels, and the channels branch out near the inlet and merge into one another towards the outlet.

In Fig. 13, we show the velocity field of the topology obtained for $w = 0$ (shown in Fig. 12). The pressure drop predicted by the Darcy flow and RANS models are 37.0 Pa and 61.6 Pa, respectively. From Fig. 13, we can see that the velocity fields computed by the Darcy and the RANS model are in a reasonable agreement with each other. More importantly, unlike for the topologies obtained when the maximum length scale was not used, there is no recirculation in the design. As a result, the discrepancy between the temperature field (shown in Fig. 14) computed using the Darcy flow and RANS models in not as severe as observed when the maximal length scale constraint was not used. The average temperature T_{av} for the Darcy flow and RANS models are 5.0 °C and 7.7 °C, respectively.

In Fig. 15, we show the velocity field of the topology obtained for $w = 0.8$ (shown in Fig. 12). The pressure drop predicted by the Darcy flow and RANS models are 51.5 Pa and 82.4 Pa, respectively. From Fig. 15, we can see that there exists a reasonable agreement between the Darcy and the RANS flow fields, and there is no recirculation in the

Table 2 The average temperature T_{av} and pressure drop P_d in Pa for the baseline and the optimized designs

	T_{av} in °C			P_d in Pa		
	RANS	Darcy	Error	RANS	Darcy	Error
Baseline	14.5	6.7	116%	27.1	27.1	—
No length scale constraint; $V_0 = 50\%$						
$w = 0$	840.7	52.9	1498%	19.0	16.1	18%
$w = 0.4$	2470.7	7.9	31056%	16.2	18.4	12%
$w = 0.8$	134.9	5.0	2598%	24.3	20.9	16%
No length scale constraint; $V_0 = 20\%$						
$w = 0.7$	15.3	12.8	20%	46.6	43.1	8%
$w = 0.8$	12.0	10.7	12%	49.4	52.4	6%
$w = 0.9$	9.3	8.5	9%	65.4	55.3	18%
Length scale constraint $r_{max} = 3.12$ cm; $V_0 = 50\%$						
$w = 0.0$	7.7	5.0	55%	61.6	37.0	67%
$w = 0.4$	6.0	4.6	29%	62.1	37.1	67%
$w = 0.8$	4.4	4.5	3%	82.4	51.5	60%

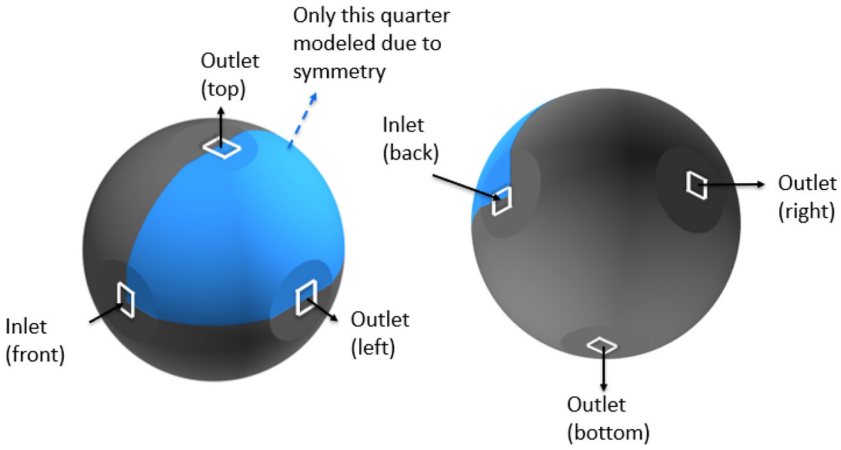

Fig. 17 Schematic of the domain hollow sphere, with two inlets on its front and back faces and four outlets on its left, right, top and bottom faces

design. As a result, there is very little discrepancy between the temperature field (shown in Fig. 16) computed using the Darcy flow and RANS models. The average temperature T_{av} for the Darcy flow and RANS models are 4.4 °C and 4.5 °C, respectively.

From Figs. 13 and 15, we can see that imposing the maximum length scale constraint clearly eliminated the recirculation in the topology, and improved the correlation between the Darcy flow and RANS solutions. Moreover, the difference in the average temperature values predicted by the Darcy flow and RANS solutions decreased as the weighting factor w increased. Therefore, from this investigation, we can clearly see that the designs obtained with narrow channels have a significantly better correlation between the Darcy and RANS flow fields and temperature fields, compared with the design obtained with wider channels.

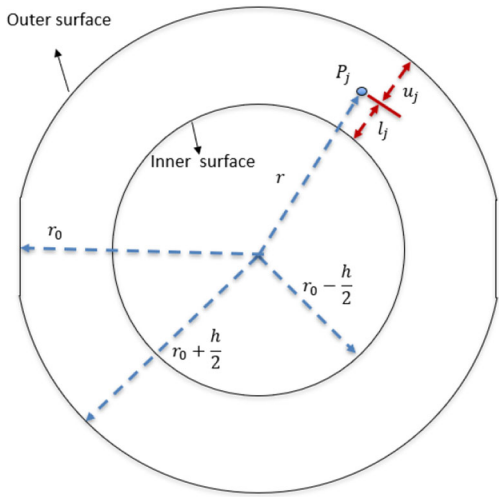

Fig. 18 Schematic of the sphere illustrating the computation of the bounds for a boundary point P_j for conforming the topology to the sphere

Table 2 shows the pressure drop P_d and the average temperature values for the baseline design, the different optimized topologies. The permeability constant used in the Darcy flow model is computed in such a way that the pressure drops predicted by the Darcy flow and RANS model match for the baseline design. From Table 2, we can see that when length scale constraint is not used, and a volume fraction constraint of $V_0 = 50\%$ is used, the resulting designs are significantly inefficient in terms of their cooling performance. Specifically, the average temperatures predicted by the RANS flow are more than two orders of magnitude higher than the Darcy flow predictions. The pressure predictions, however, are in a reasonable agreement with each other, with the errors less than 20%.

On the other hand, when the volume fraction constraint is decreased to $V_0 = 20\%$, the discrepancy between the Darcy and the RANS simulation is significantly reduced. The observed maximum length scale for the designs is a low, 2.65 cm, therefore leading to a better agreement. Moreover, the average temperature for $w = 0.8, 0.9$ is lower than the baseline design (which has a volume of 50%), but the average temperature for $w = 0.7$ is higher than that of the baseline. Furthermore, the error between the average temperature predicted by both the models decreases as w increases. For the case with $w = 0.9$, the error is a as low as 9%. The error in pressures is also in a reasonable agreement, with the errors less than 20%.

When the length scale constraint of $r_{max} = 3.12$ cm is used, the Darcy and the RANS flow fields are in a reasonable agreement. The Darcy flow model under-predicts the pressure and temperature values, by over 60%. The error between the average temperature predicted by both the models decreases as w increases. For the case with $w = 0.8$, the error is a low, 3%. More importantly, all the designs have efficient cooling performance, with the average temperatures in the design significantly lower than the baseline design, however, at the cost of higher pressure drops.

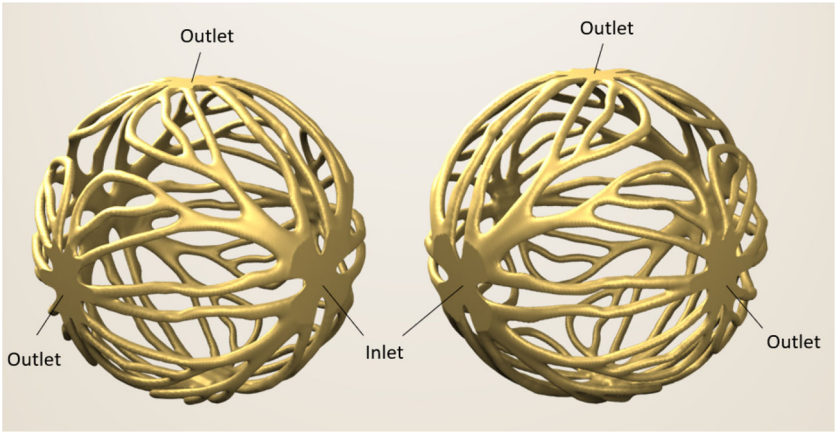

Fig. 19 Optimized results of the cooling channels conforming to the surface of the sphere

From this investigation, we can conclude that the Darcy flow model can be used effectively to design the topologies with narrow channels that distribute the flow appropriately so as to minimize the average temperature in the domain.

4 Design of conformal cooling channels

Conformal cooling channels are used to improve the cooling performance in plastic injection molding, where the channel follows the shape of the surface of the mould core (Dimla et al. 2005). In this section, we show an example of using topology optimization in the design of cooling channels conforming to the surface of a hollow sphere. In Fig. 17, a schematic of the domain of a hollow sphere is shown, where the sphere is truncated at six places so as to form flat surfaces for the fluid to enter and exit the domain. The bounding box of the sphere is a cube of side length d = 0.5 m. The sphere has two inlets (5.0 cm $\times$ 5.0 cm each) on its front and back faces face and four outlets (5.0 cm $\times$ 5.0 cm) on the other faces. The fluid is coming through the inlets with a velocity of 0.2 m/s and $T = 0$ °C. The sphere is $h = 12.5$ mm thick and is subjected to a volumetric heating of 10^7 W/m^3. Due to the symmetry, only a quarter of the domain is modeled using an FE mesh of 160 $\times$ 80 $\times$ 80 elements, using regular cubic elements. The Reynolds number based on the inlet width is 10^4. In the previous section, we demonstrated that if the volume constraint is low, then the obtained topologies can comprise of narrow channels so as to avoid recirculation. Therefore, we set the volume constraint used to be a low $V_0 = 3\%$, for the design of the conformal channels, and we do not use the maximum length scale constraint.

The topology of the flow channels are made to conform to the sphere by imposing lower and upper bound constraints (l_j and u_j in Eq. 36) on the boundary points movement. A schematic of the sphere illustrating the computation of the lower and upper bounds, l_j and u_j, of a boundary point P_j is shown in Fig. 18. The radius of the outer surface of the sphere is $r_0 + h/2$ and the inner surface has a radius of $r_0 - h/2$, where $r_0 = d/2 = 0.25$ m is the radius of the centerline of the sphere. r is the distance from a boundary point P_j to the center of the sphere. The upper bound u_j is the distance from the boundary point P_j to the outer surface; and the lower bound l_j is the distance from the boundary point P_j to the inner surface given by

$$l_j = r_0 - h/2 - r; \quad u_j = r_0 + h/2 - r \tag{38}$$

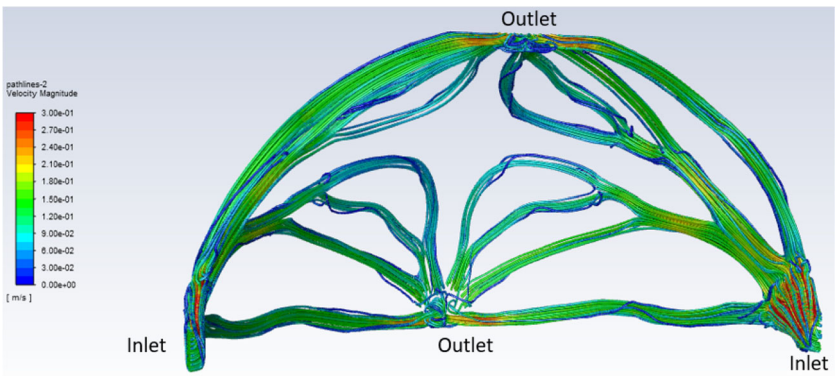

Fig. 20 The pathlines illustrating the RANS flow computed in Ansys Fluent for a quarter of the optimized cooling channel

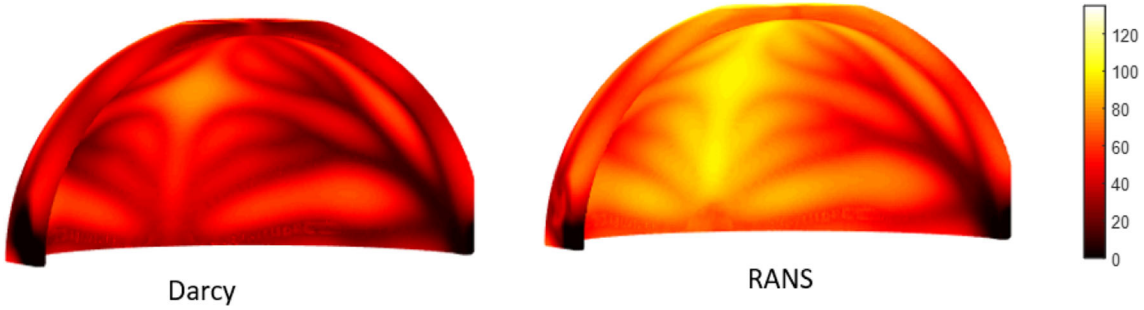

Fig. 21 Temperature distribution on the surface of the sphere in °C computed using the Darcy and RANS flow fields

The optimization process is performed for 100 iterations which takes approximately 1.5 h to complete. Figure 19 shows the optimized results obtained for $w = 0.8$, where we can see that the channels branch out from the inlet, distribute themselves over the surface of the sphere before merging back near the outlets. A quarter of the optimized topology shown in Fig. 19 is post-processed in Ansys Fluent with a RANS model for comparison. Figure 20 shows the pathlines of the flow colored by the magnitude of the velocity. The pressure drop predicted by the Darcy and RANS flow are 276 Pa and 166 Pa, respectively. Figure 21 shows the temperature distribution on the surface of the sphere. The average temperature predicted by the RANS model is 66.1°C. The Darcy flow predicts a more uniform distribution of the flow on the sphere, and as a result, it predicts a lower values of temperatures on the surface, with the average temperature being 41.8°C.

5 Conclusions

This paper introduces a level set topology optimization method for 2D and 3D problems considering convective heat transfer. The linear Darcy potential flow is used to simulate the flow and the heat transfer is modeled by the convection-diffusion equation using the finite element method. The pressure drop and the average temperature are minimized subject to a volume constraint and a length scale constraint. The level set topology optimization algorithm is applied to the design of cooling channels. The obtained topologies are post-processed in Ansys Fluent with a high fidelity RANS model. The pressure drop and average temperature predicted by the RANS and Darcy flow models are compared.

The results obtained in the absence of the maximum length scale constraint show that, as the weighting factor for the temperature increases, the flow is distributed more evenly, effectively cooling down the structure, at the cost of the higher pressure drops. However, there was a significant discrepancy between the the Darcy and the RANS flow fields, primarily due to the presence of wide channels, resulting in highly inefficient cooling performance. When the volume constraint was decreased, the optimized topologies featured narrower channels, and there was very little discrepancy between the Darcy and the RANS flow fields, resulting in efficient cooling performance. The resulting average temperature of the designs obtained for the weighting factor $w \geq 0.8$ designs had lower values of average temperature than the baseline design.

The results obtained with the maximum length scale constraint show that, for the obtained optimized topologies, there was a reasonable agreement between the RANS and Darcy flow models, resulting in efficient cooling performance. The resulting average temperature of the obtained designs had lower values than that of the baseline design. Therefore, by restricting the design space to narrow channels, we successfully optimized the cooling performance and sufficiently captured the turbulent flow physics using the low fidelity Darcy flow model.

Finally, the design of conformal cooling channels on the surface of a sphere using topology optimization is presented. The results show that the channels organically branch out from the inlets, distribute themselves over the surface of the sphere before merging back near the outlets, effectively cooling the surface of the sphere. There was a reasonable agreement between the RANS and Darcy flow models, resulting in efficient cooling performance.

Acknowledgments We would like to thank the anonymous reviewers and the handling editor, Prof. Ole Sigmund, for their insightful comments that greatly improved the manuscript.

Funding information The authors acknowledge the support from DARPA (Award number HR0011-16-2-0032) and NASA Transformational Tools and Technologies (TTT) project (grant number 80NSSC18M0153).

Compliance with ethical standards

Conflict of interest The authors declare that they have no conflict of interest.

Replication of results The supplementary material provided the Ansys Fluent case and data files for the baseline design and the optimized 2D designs obtained for $w = 0.8$.

References

Arora JS (2004) Introduction to optimum design. Elsevier, Amsterdam

Asmussen J, Alexandersen J, Sigmund O, Andreasen CS (2019) A "poor man's" approach to topology optimization of natural convection problems. Struct Multidiscip Optim 59(4):1105–1124

Borrvall T, Petersson J (2003) Topology optimization of fluids in stokes flow. Int J Numer Methods Fluids 41(1):77–107

Dilgen CB, Dilgen SB, Fuhrman DR, Sigmund O, Lazarov BS (2018a) Topology optimization of turbulent flows. Comput Methods Appl Mech Eng 331:363–393

Dilgen SB, Dilgen CB, Fuhrman DR, Sigmund O, Lazarov BS (2018b) Density based topology optimization of turbulent flow heat transfer systems. Struct Multidiscip Optim 57(5):1905–1918

Dimla D, Camilotto M, Miani F (2005) Design and optimisation of conformal cooling channels in injection moulding tools. J Mater Process Technol 164:1294–1300

Dunning PD, Kim HA, Mullineux G (2011) Investigation and improvement of sensitivity computation using the area-fraction weighted fixed grid fem and structural optimization. Finite Elem Anal Des 47(8):933–941

Dunning PD, Kim HA (2015) Introducing the sequential linear programming level-set method for topology optimization. Struct Multidiscip Optim 51(3):631–643

Gersborg-Hansen A, Sigmund O, Haber RB (2005) Topology optimization of channel flow problems. Struct Multidiscip Optim 30(3):181–192

Guest JK, Prévost JH (2006) Topology optimization of creeping fluid flows using a darcy–stokes finite element. Int J Numer Methods Eng 66(3):461–484

Hu P, He B, Ying L (2016) Numerical investigation on cooling performance of hot stamping tool with various channel designs. Appl Therm Eng 96:338–351

Jahan S, Wu T, Shin Y, Tovar A, El-Mounayri H (2019) Thermo-fluid topology optimization and experimental study of conformal cooling channels for 3d printed plastic injection molds. Procedia Manuf 34:631–639

Koga AA, Lopes ECC, Nova HFV, De Lima CR, Silva ECN (2013) Development of heat sink device by using topology optimization. Int J Heat Mass Transfer 64:759–772

Kontoleontos E, Papoutsis-Kiachagias E, Zymaris A, Papadimitriou D, Giannakoglou K (2013) Adjoint-based constrained topology optimization for viscous flows, including heat transfer. Eng Optim 45(8):941–961

Pollini N, Sigmund O, Andreasen CS, Alexandersen J (2020) A "poor man's" approach for high-resolution three-dimensional topology design for natural convection problems. Adv Eng Softw 140:102736

Qiao H (2006) A systematic computer-aided approach to cooling system optimal design in plastic injection molding. Int J Mech Sci 48(4):430–439

Sethian JA (1999) Level set methods and fast marching methods: evolving interfaces in computational geometry, fluid mechanics, computer vision, and materials science, vol 3. Cambridge University Press

Sethian JA, Vladimirsky A (2000) Fast methods for the eikonal and related hamilton–jacobi equations on unstructured meshes. Proc Natl Acad Sci 97(11):5699–5703

Tan MHY, Najafi AR, Pety SJ, White SR, Geubelle PH (2016) Gradient-based design of actively-cooled microvascular composite panels. Int J Heat Mass Transfer 103:594–606

Wang G, Zhao G, Li H, Guan Y (2011) Research on optimization design of the heating/cooling channels for rapid heat cycle molding based on response surface methodology and constrained particle swarm optimization. Expert Syst Appl 38(6):6705–6719

Wu J, Aage N, Westermann R, Sigmund O (2017) Infill optimization for additive manufacturing—approaching bone-like porous structures. IEEE Trans Vis Comput Graph 24(2):1127–1140

Wu T, Tovar A (2018) Design for additive manufacturing of conformal cooling channels using thermal-fluid topology optimization and application in injection molds. In: ASME 2018 International design engineering technical conferences and computers and information in engineering conference, pp v02BT03a007–v02BT03a007. American Society of Mechanical Engineers

Yaji K, Yamada T, Kubo S, Izui K, Nishiwaki S (2015) A topology optimization method for a coupled thermal–fluid problem using level set boundary expressions. Int J Heat Mass Transfer 81:878–888

Yoon GH (2010) Topological design of heat dissipating structure with forced convective heat transfer. J Mech Sci Technol 24(6):1225–1233

Yoon GH (2016) Topology optimization for turbulent flow with spalart–allmaras model. Comput Methods Appl Mech Eng 303:288–311

Zhao X, Zhou M, Sigmund O, Andreasen CS (2018) A "poor man's approach" to topology optimization of cooling channels based on a darcy flow model. Int J Heat Mass Transfer 116:1108–1123

Zhao X, Zhou M, Liu Y, Ding M, Hu P, Zhu P (2019) Topology optimization of channel cooling structures considering thermomechanical behavior. Struct Multidiscip Optim 59(2):613–632